

P. Scavella¹, G. Paolillo¹, T. Astarita¹, G. Cardone¹ & C.S.Greco¹

¹Department of Industrial Engineering, University of Naples "Federico II", Naples, Italy

Abstract

Active flow control is a promising solution for green aviation, reducing environmental impact, noise, and costs while enhancing reliability and Low-Speed performances addressing the global growth in air mobility. This study numerically assesses, by beans of RANS simulation, Circulation Control (CC) technology applied on a two-dimensional airfoil, focusing on a no-moving-parts design to lower costs and weight. Various Coanda airfoil configurations are evaluated, with the best-rounded trailing edge compared to the Co-Flow jet and traditional slotted flap. Coanda airfoils show superior performance, achieving higher lift at lower angles of attack and reducing drag, beneficial for Short Takeoff and Landing (STOL) aircraft. A parametric study on the elliptical trailing edge highlights key aerodynamic factors. A three-dimensional analysis confirms CC wings offer more lift than slotted flaps but with higher drag due to increased vorticity. Optimizing the blowing distribution to achieve a regular wing loading can mitigate lift-induced drag giving way to very efficient and flexible lifting surfaces.

Keywords: High Lift Systems, Flow Control, Circulation Control

1. Introduction

Since the need for new disruptive technology for green aviation became more and more stringent a particular focus on aerodynamic performance to enhance overall flight efficiency is ever increasing. Many strategies could be useful to achieve better aerodynamics which can operate at a higher level, designing novel aircraft architectures or operating on individual phases of the flight envelope, maintaining the concept of change of configuration.

Even though numerous architecture concepts have been conceived to face the environmental impact and to increase the overall performance (*e.g.* Blended wing body, HARWs, non-planar wing, ... [1]), a completely new aircraft architecture is a much more difficult challenge than a focused endeavor on a specific aspect.

Extreme focus is dedicated to low-speed operation due to the principal role in addressing the global growth in air mobility especially for its transformation to door-to-door transportation. Shortening the take-off and landing distance for the sake of operating also on very short runways is the challenge. Reducing airport noise is another challenge to overcome to guarantee a sustainable connection to customers in populated areas in order to maximize aviation's potential as a modern means of transportation. Special attention is given in [2] on high lift systems integrated into a new class of airplanes that are able to deal with low noise impact, short take-off and landing while maintaining high cruise efficiency as well.

In [3] the smaller regional aircraft are considered the key candidates for future commercial aviation because their role will be strengthened by their capacity to face the STOL requirements, for reducing DOC, noise emission and lower fuel consumption [2]. C. Courtin *et al.* in [4] evidences eSTOL aircraft as a viable path for Urban Air Mobility (UAM) network with significant advantage with respect to vehicle payload and certification risk. Runway length as short as 100-300 ft could be achieved with a proper short field performance (maximum lift coefficient and flight path angle).

Indeed, the low-speed operations are mainly influenced by High-Lift systems due to their peculiarity in reducing the lowest flight speed of the envelope, thus the STOL requirements can be met by operating on their design. A good high-lift design is also crucial for maintaining an affordable wing loading for high cruise efficiency [5], and lower susceptibility to turbulence [6]

The term "Low-Speed" can be misleading [7] as it often refers to slow flows at a few meters per second where friction forces are significant. In High-Lift Aerodynamics, low speeds are relative to the cruising speeds of aircraft, with landing flow velocities ranging from 30 kts for small planes to 200 kts for large transport aircraft.

High-lift systems are significant contributors to airplane costs [8]. A trailing edge (TE) high lift system represents 2.5 % to 6.4% of manufacturing costs, while a leading edge (LE) device accounts for 1.5% to 3.4%, totaling 6% to 11% of the production cost.

P.T.Meredith in [9] highlights the importance of increasing the maximum lift coefficient for carrying more passengers, the improvement of lift-to-drag ratio to increase payload, and how the shift upwards of the lift curve has a strong effect on the reduction of attitude for a given glideslope angle. Wimpress in [10] conveys that small aerodynamic improvements can significantly enhance airplane utility and profitability. For instance, a 5% increase in maximum lift coefficient could boost payload by 20% and operator profit per flight by 40%.

Therefore, considering a more promising and flexible solution for a high lift system rather than the classical multi-element systems could have a relevant leverage on the overall aircraft performance. Circulation Control technology has been always considered to have great potential to be a suitable system for the flexibility needed to overcome the coexistence of cruise efficiency, noise reduction, and STOL capabilities. Kweder *et al.* [11] highlight the main benefit of using circulation control on fixed-wing aircraft: limited or even no actuation systems for moving control surfaces are needed; Control circulation serves as direct lift control independently of the angle of attack; Jet turning angles are no longer limited by physical jet exit angle or flap deflection; Very high force augmentation can be achieved per unit blowing momentum input.

1.1 Circulation Control

Circulation in potential flows is solely controlled by the superposition of the Kutta condition, more specifically by the positioning of the stagnation points (s.ps.). Target flow fields for high-lift applications occur when the two stagnation points merge on the lower surface of the body¹ fully exploiting the lift potential flow limit [12].

In viscous flow fields, provided the absence of significant flow separation, the Kutta condition is a reflection of viscous flow approaching geometrical discontinuities towards the rear part of the body. Indeed, only in viscous flow, real lift and drag forces appear in aerodynamics bodies flow [13].

However, bodies immersed in viscous flow fields may experience flow separation in specific conditions, hence the positioning of geometrical discontinuity no longer serves the purpose of defining circulation. The possibility of leveraging flow control to avoid flow separation may give way to dedicated circulation-control geometries with the final aim of uniquely controlling the s.p. on the lower surface of the body.

As explained in [12], the problem of modifying circulation has to be thought from the modification of the rear stagnation point (s.p.) of potential non-lifting flow: no circulation is present when the s.p. is on the upper surface, and as this point shift backward to the T.E. to meet Kutta condition an increase of circulation will occur. Continuing on this line, any forward shifting of the s.p. on the lower surface is equivalent to an increasing circulation.

Once flow control is used to avoid separation on the upper surface of lifting bodies due to severe pressure gradient or geometrical discontinuities, the elimination of that T.E. discontinuity is necessary to move the rear stagnation point on the lower surface in the forward direction with the final goal of enhancing circulation. Here is the birth of the rounded trailing edge airfoil, where a tangential jet is introduced through a blowing slot to overcome adverse pressure gradients. Depending on the blowing effort, the flow will be capable of turning around the regular T.E. moving proportionally forward the separation point. The jet causes the boundary layer and the jet sheet to remain attached along

¹Further improvements on the circulation around the body are achieved by forcing the s.p. outside the body.

the curved surface for the entrainment effect[14]. This observable physics phenomenon is generally recognized as the Coanda Effect [15, 16]. The balance of centrifugal and pressure forces across the curved flow causes low pressure, enhancing viscous and turbulent diffusion downstream from the blowing slot thus causing wake spreading. This final effect that serves to enhance lift capabilities is the effect of curving external irrotational flow streamline. A specific design space for efficient Coanda surface exists [17] in terms of slot height to radius ratio h_j/r and slot height to chord ratio h_j/c . Small and high-velocity jets cannot cause the right entrainment hence they cause only a local modification to the flow field without curving the outer streamline, while thicker and lower-velocity jets have problems with facing separation.

Even though a rounded trailing edge has been proven to perform well and retain the fashion of the lack of moving parts, drag problems arise when this airfoil deals with cruise operations. Hence, as well as the classical multi-element system, the concept of change of configuration remains to combine cruise efficiency and circulation control capabilities in low-speed operations (e.g. dual radius flap [18] or movable trailing edge [3]) or use continuous blowing in cruise condition. Remaining on the concept of reducing complexity and weight during high-lift system design by avoiding the use of moving parts, CoFlow Jet (CFJ) is a valuable flow control technique with potential in both low and high-speed operations.

Zha and Paxton in [19] proposed the CFJ airfoil that is characterized to have effectiveness, energy efficiency, and ease of implementation. The CFJ airfoil involves the opening of an injection slot near the leading edge and a suction slot near the trailing edge on the suction surface of the airfoil. This opening is achieved by translating a substantial portion of the suction surface downward. Subsequently, a high-energy jet is tangentially injected near the leading edge, and an equivalent mass flow is simultaneously drawn near the trailing edge. The turbulent shear layer formed between the main flow and the jet results in robust turbulence diffusion and mixing. This enhances lateral energy transport from the jet to the main flow, enabling the main flow to overcome severe adverse pressure gradients and remain attached at high angles of attack. Through experimental analysis and CFD simulations [19, 20, 21, 22, 23], it has been demonstrated that the co-flow jet airfoil can significantly enhance lift, reduce drag, and increase stall margin. Moreover, the CFJ airfoil has the capability to recirculate the jet mass flow (zero net mass flux), thereby substantially reducing the penalty to the propulsion system by avoiding the dumping of the jet mass flow. Through CFD simulations, H. Zhi et al. in [24] demonstrate the effectiveness of incorporating basic high-lift devices into a CFJ airfoil for improved low-speed take-off and landing performance, identifying that careful selection of injection and suction slot locations, rather than the angle of the suction slot, significantly enhances lift and efficiency. Their findings support the CFJ airfoil as a practical choice for achieving short take-off and landing at small angles of attack even though a coupling with a source of circulation is present.

This technology is presented as a modified airfoil with more significant efficiency: the slight increase in circulation due to the jet is the secondary effect, whereas the delayed separation is one of the primary impacts, and its advantage could be only exploited at a high angle of attack, generating a super lift coefficient for relatively high jet coefficient [25]. A. Lefebvre, G.-C. Zha [26] propose a small electric aircraft design with high cruise efficiency due to high wing loading which is possible by the use of CFJ combined with a rotatable wing around a pivot activated during take-off and landing. Even though a great lift coefficient of 4.8 is achieved with $25 \ deg$ pivot wing angle, the application of this design to a general aviation aircraft is still a challenge due principally to structural and safety limitations.

The latter solution is a direct consequence that the typical wing angle in high lift operation is not so high to reach the maximum lift coefficient angle. R.J. Englar *et al.* in their analysis [27] highlight that a proper assumed landing and take-off operational angle of attack for evaluating low-speed performances are about 1 deg and 8 deg respectively ground roll and liftoff for take-off and 1 deg and 6 deg for landing ground roll and approach phase. Indeed classical multi-element mechanical system serves to increase overall wing curvature increasing circulation even at relatively small angles of attack. The influence of the maximum lift coefficient is reflected in the stall speed (also from regulation specification) and from stall speed came rotation speed which is responsible for the ground roll phase ending. Powered take-off analysis using a circulation control system as high-lift device is carried out

[28], in which the author points out that a more realistic criterion to determine when the rotation occurs must not depend only on $C_{L,max}$ but from the ratio between the $C_{L,rotation}$ and $C_{L,max}$. Here the ability of circulation control to mimic curvature and have superior lift performance at a typical rotation angle of attack (or approach angle), serves to make STOL technology possible. This work, employing numerical analysis, explores some possible 2D Circulation Control solutions, focusing attention on the best one by analyzing its aerodynamic performance on a finite wing.

2. Numerical Setup and Validation

Circulation Control devices have been developed in many from, without geometrical discontinuities like elliptical or circular shapes, or as a modification by cambering the original airfoil. Even though for different reasons, all these different shapes have to deal with separation. The circulation that this device is capable of generating is one of characterizing performance and it is strongly dependent on where the separation occurs. Therefore the accuracy and robustness of the separation point prediction are crucial for determining a reliable index that can identify a well-designed geometry. Many numerical investigations have been done on validation of CFD code and turbulence models for RANS [29, 30, 31, 32] and LES [33, 34]. Taking into account the curvature and rotation effect seems to be a good practice for using RANS modeling, like Spalart Allmaras (SA) which naturally does not take into account this effect directly. With that correction, the simulation yields near results compared with experimental evidence for a low blowing coefficient C_{μ} .

Several previous works are used to verify the numerical setup. Fluent is used as a solver with both compressible and incompressible RANS solutions. Both structured and unstructured mesh approaches are used with over 5 million nodes. Rumsey and Nishino in [34] take under analysis the *CC-E0020EJ* elliptical airfoil from which several cases are studied: starting studying the effect of grid size, to the effect of using Curvature correction on RANS turbulent modeling and finally, LES calculation is performed on the same geometry. To assess if SA and SARC (SA with rotation and curvature correction) turbulence models in Fluent give acceptable results compared with the ones from the paper, the same mesh and boundary conditions are used. Figure 2 reports the velocity contours on the Coanda surface depicting the separation point: a separation angle of $\phi_s = 70 \ deg$ is measured from the jet inlet, while for the same conditions, a $\phi_s = 73 \ deg$ are calculated in the paper. Table 1 reports the comparison of lift coefficient using two turbulence models SA and SARC and the result obtained by the authors for two different blowing coefficients C_u .

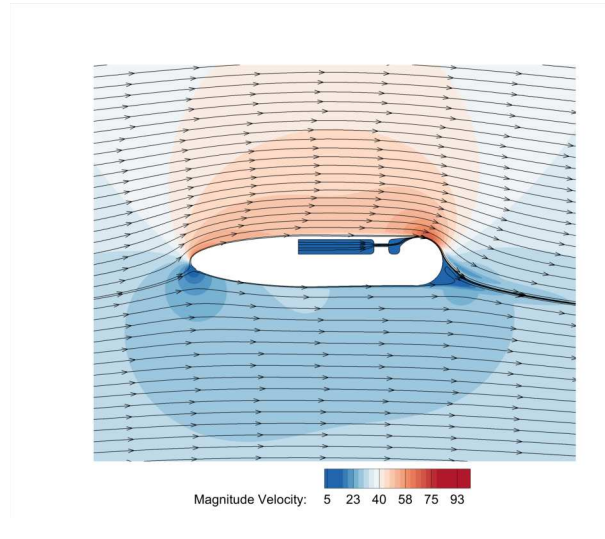


Figure 1. Velocity contours and streamline on airfoil from [34], $\alpha = 0$ deg, $Re = 4.89 \times 10^5$, M = 0.1, $C_{tt} = 0.044$.

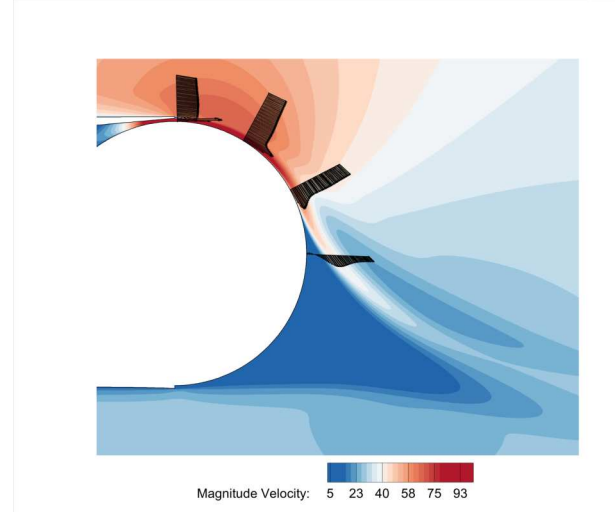


Figure 2. Zoom on Coanda surface 1, separation point occurs at an angle of about 70 *deg* compared to 73 *deg* from [34]

Swanson *et al.* [31, 32] computed solutions for the CC airfoil flows of the Novak *et al.* [35] experiment. They solved the RANS equations using several turbulence models (SA, SARC, SST) and several grid densities to determine their effects on the solution. They utilize the wind tunnel correction from the initial wind tunnel experiment because its influence is significant due to the high circulation.

	SA	SA[34]	SARC	SARC [34]
$\overline{C_{\mu} = 0.044}$	1.87	1.84	1.84	1.72
$C_{\mu} = 0.12$	4.67	4.65	4.49	4.04

Table 1. Comparison with [34] using Fluent with the same mesh and boundary conditions. The constant of RC correction is C = 1.

They highlight that the use of curvature correction in the turbulence models leads to a much similar pressure distribution and streamlines with respect to the experiments. Figure 3 reports the velocity contours calculated with the SARC model ($C_{curv=20}$) at the corrected angle of attack for wind tunnel effect $\alpha=-5.86$ deg correspondent to $\alpha=0$ deg at $C_{\mu}=0.1$. The pressure coefficient is reported in figure 4 and compared with the experimental one: the irregularity of the calculated one is due to the difficulty of replicating exactly the geometry. Table 2 reports the lift coefficient for both blowing conditions, obtained with the SA model and several curvature corrections. Depending on the correction the experimental values seem to have a better match with the prediction rather than the classic SA model. Figure 5 reports the streamline near the Coanda surface in several cases. The results obtained with curvature correction have similar separation point angles with respect to the experimental one [35], indicated by the arrow. The results relative to curvature correction give a better agreement with separation angle, more evident in higher blowing case ((a) and (b) in fig. 5)

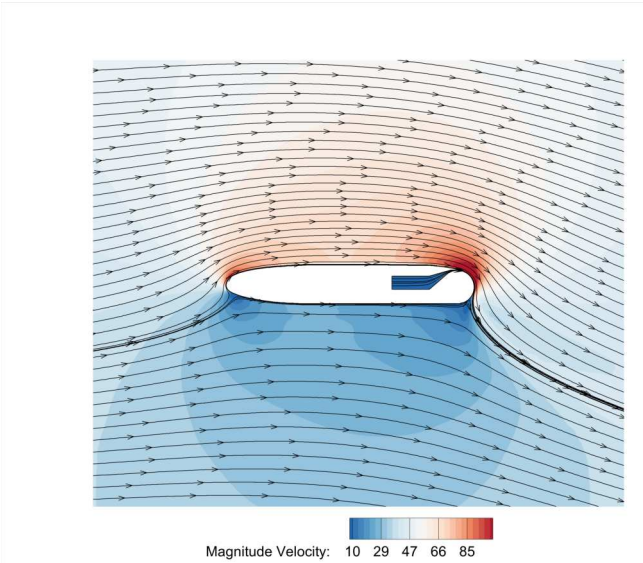


Figure 3. Velocity contours and streamline on airfoil from [32], $\alpha = -5.86$ deg, $Re = 0.98 \times 10^6$, M = 0.12, $C_{\mu} = 0.1$.

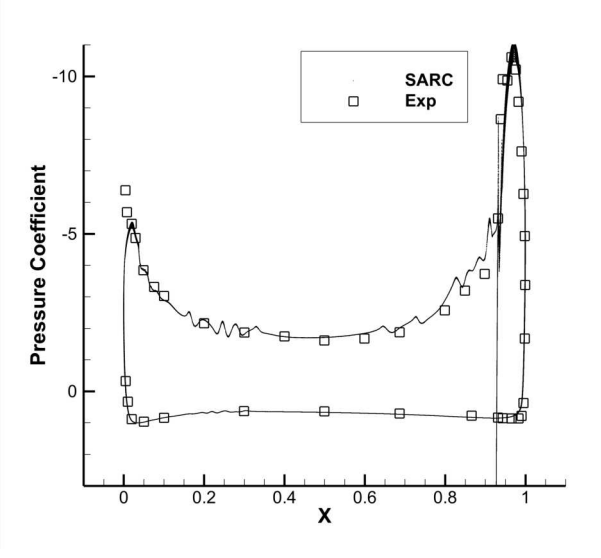


Figure 4. Pressure coefficient in conditions of figure 3 calculated with SARC model compared with the experimental data from [35, 32]

	C_{μ}	SA	$C_{curv} = 1$	$C_{curv} = 5$	$C_{curv} = 15$	$C_{curv} = 20$	exp
C	0.03	1.684	1.811 4.325	1.702	1.460	1.409	1.5
c_l	0.1	4.674	4.325	4.644	3.841	3.686	3.575

Table 2. lift coefficient on airfoil from [31] depicted in figure 3, with several curvature correction constants compared with the experimental values.

Even though the correct C_{curv} is unknown a priori, the result using that correction shows a better correlation with experimental evidence and this is more valid the weaker the blowing is. Other two cases are taken into consideration for validating the numerical setup: moving to a smaller T.E. radius like the GACC airfoil from [36]. An O-type structured mesh is generated (fig. 6) and the SA turbulence model is used in Fluent. The calculations are performed by fixing the angle of attack to zero and the

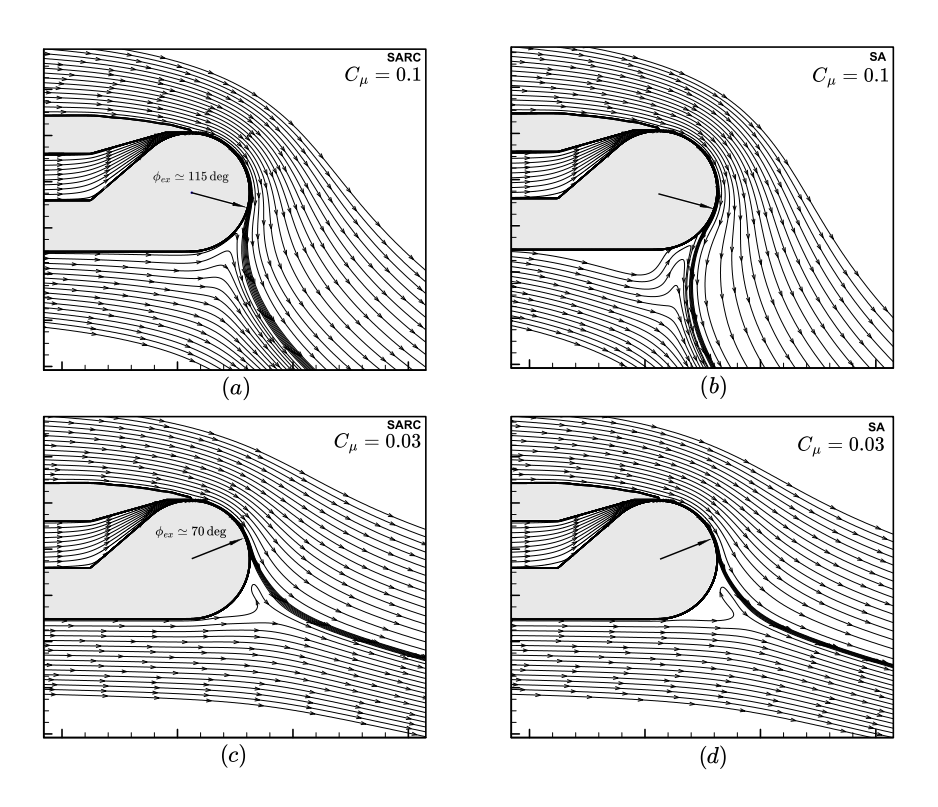


Figure 5. Steamline obtained with curvature correction (left side (a) and (c)) and classic SA ((b) and (d)) in two different blowing conditions: $C_{\mu} = 0.1$ (a),(b) and $C_{\mu} = 0.1$ (c),(d).

Reynolds number $Re = 0.5 \times 10^6$ corresponding to a free stream velocity $U_\infty = 30~ms^{-1}$. Figure 8 depicts the lift coefficient obtained with the SA model for several blowing levels and is compared with numerical results and experimental data present in [36]. Good agreement for lift coefficient with respect to the experiment can be observed while for high blowing coefficient, they are not still coherent. The drag coefficient calculated versus the lift coefficient differs more the more the blowing level. Difficulty in matching the drag coefficient obtained numerically (also provided by [36]) and the experimental evidence must be noted.

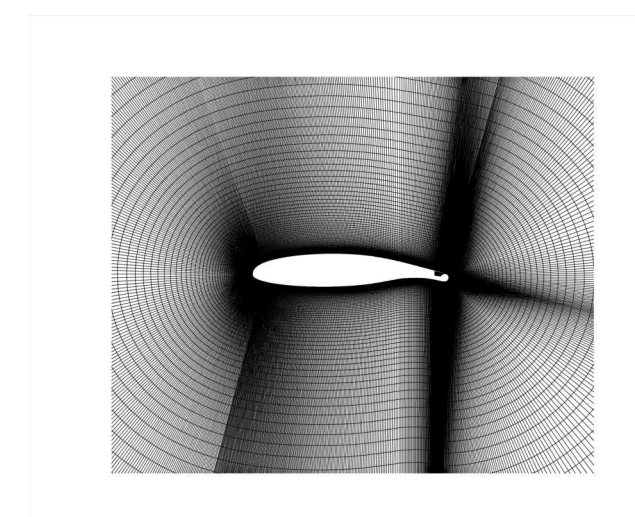


Figure 6. O-type structured mesh on GACC airfoil from [36]

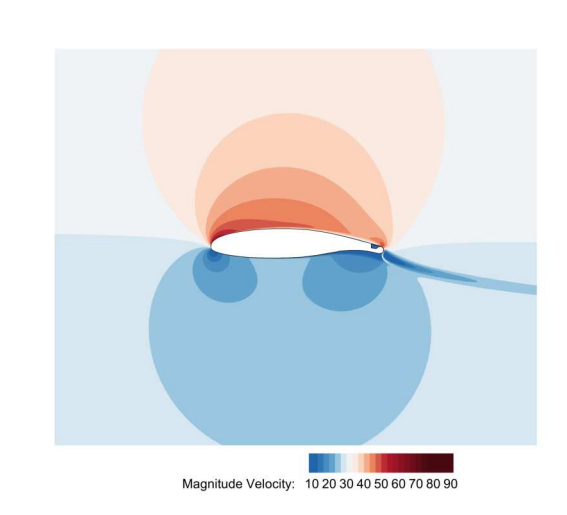


Figure 7. Velocity contour of GACC airfoil at $\alpha=0$ deg, $C_{\mu}=0.03$ and $Re=0.5\times 10^6$.

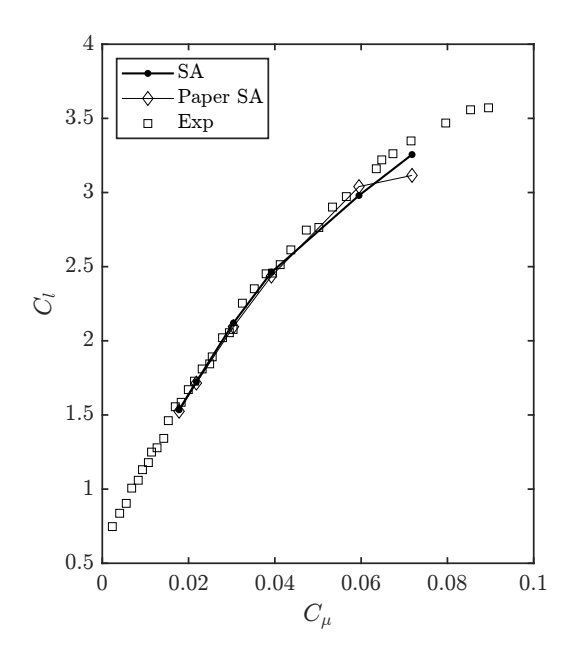


Figure 8. Lift coefficient versus the blowing coefficient, $Re = 0.5 \times 10^6$. Comparison with experimental data and numerical result form [36].

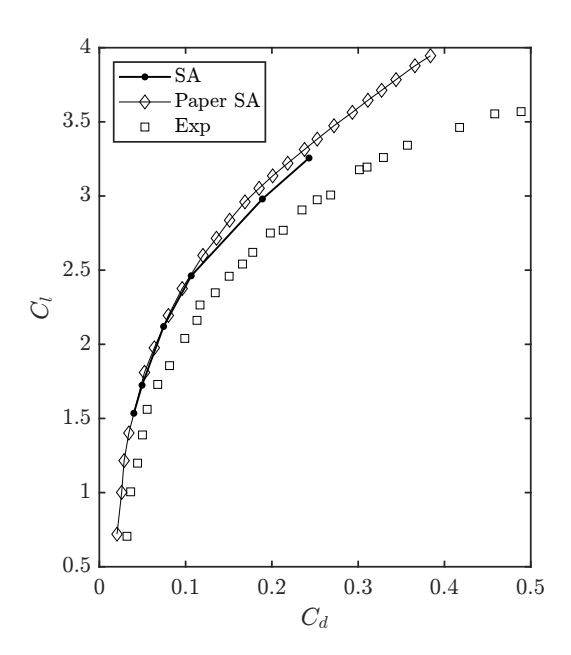


Figure 9. Lift coefficient versus the drag coefficient for increasing C_{μ} , $Re=0.5\times 10^6$. Comparison with experimental data and numerical result form [36].

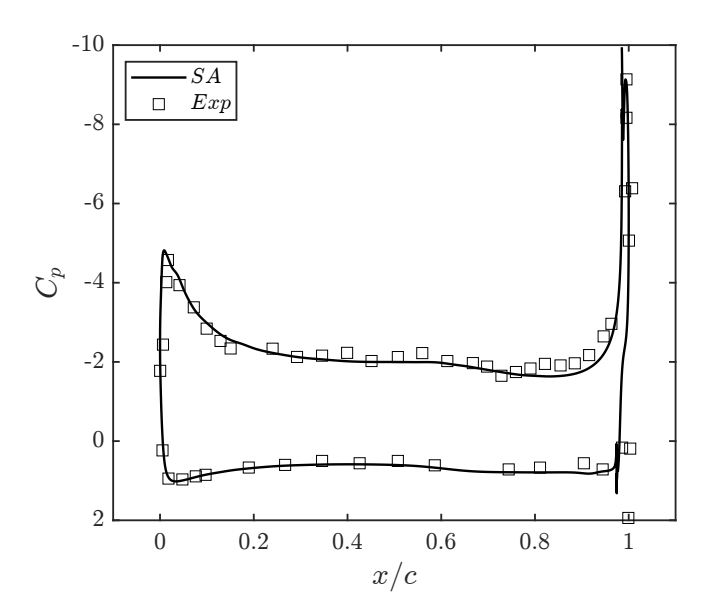
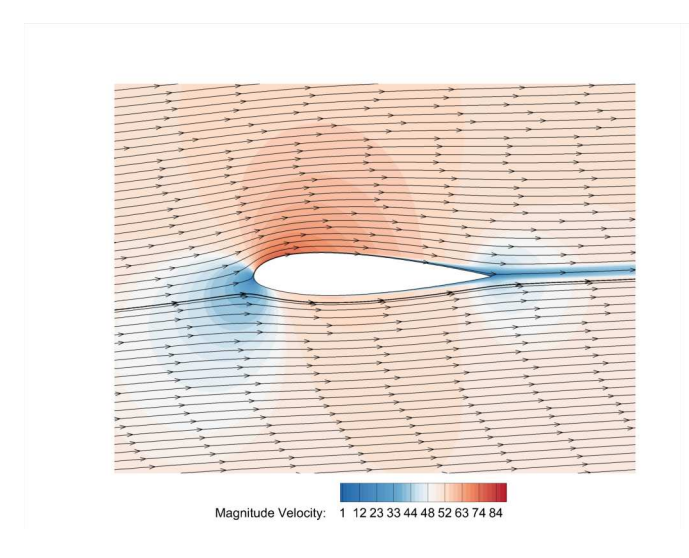


Figure 10. Pressure coefficient on GACC airfoil, $\alpha = 0$ deg, $C_{\mu} = 0.06$, $Re = 0.5 \times 10^6$.

3. Numerical Analysis

A preliminary study on fixed trailing edge shape is performed starting from a generic NACA airfoil 23015. From the blunt trailing edge, several curved geometries can be obtained by truncating it by a quantity h_{cut} . Then a circular or ellipse shape can be constructed once the slot height h_{slot} is determined (fig. 15).

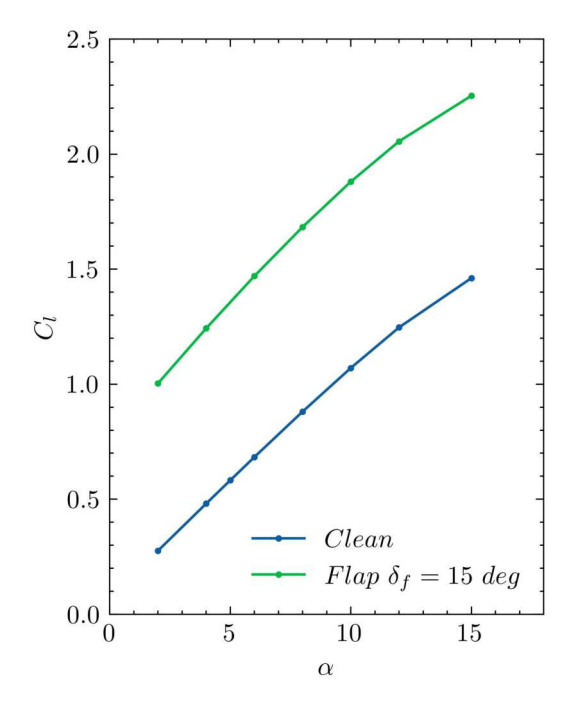
The Coanda geometries must be compared to a baseline. Thus RANS simulation with SA model is performed on the clean airfoil and a classical slotted flap high lift system to compare the performance. Velocity contours and streamline are reported in figures 11 and 12, for both the geometry at $\alpha=4$ deg. The lift coefficient curve and drag polar are reported respectively in figure 13 and figure 14 at the same Reynolds number. As expected the slotted flap increases the α_{zl} increasing the airfoil curvature.



Magnitude Velocity: 1 1223 33 44 48 52 63 74 84

Figure 11. Velocity contours and streamline on clean airfoil $Re = 3.2 \times 10^6$.

Figure 12. Velocity contours and streamline on an airfoil with a slotted flap deflected at $\delta_f = 15 \ deg, Re = 3.2 \times 10^6$.



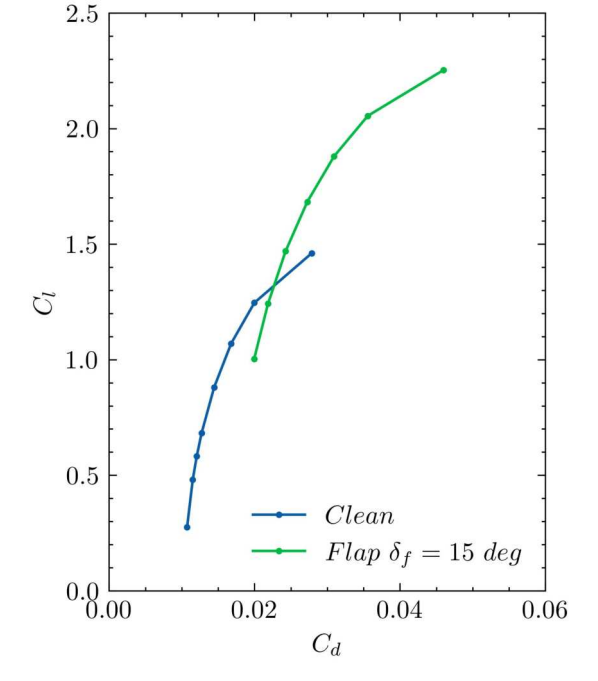


Figure 13. Lift coefficient curve, clean and flapped airfoil $Re = 3.2 \times 10^6$.

Figure 14. Drag polar comparison between clean and flapped airfoil $Re = 3.2 \times 10^6$.

The first geometry considered is a circular T.E. named 'A0' configuration where $h_{slot} = 0.2\%c$ and $h_{cut} = 0.9 \ c$. The elliptical shape differs from the geometrical construction of the rounded one: it introduces the geometrical discontinuity at T.E. which is useful for several reasons. The most important

is derived from a problem in circular geometry: if the blowing coefficient is set to a relatively high value, the flow will turn around the trailing edge going on the lower surface, creating a cushion of air directed into the inverse direction of the main flow (this happens also in [32]). This device in this particular condition creates a strong recirculation region increasing the form drag (even if decreasing the friction part) and the lift gets no benefits because the jet does not influence properly the external streamline curvature. The presence of the discontinuity permits to increase C_{μ} , with the sake of fully exploiting the potential of circulation control. Table 3 reports the preliminary geometry parameters for both circular and elliptical shapes. An O-grid mesh is generated around the airfoil as depicted in figure 16 and figure 17 respectively for A2 and B0 configuration. RANS simulations are performed with the SA turbulence model at the same angle of attack ($\alpha=4$ deg) for several blowing levels at a free stream velocity of $U_{\infty}=50$ ms^{-1} . Both configurations generate additional curvature in streamline, causing an increase of circulation. Figure 18 and 19 report respectively the velocity flow field around A0 and B0 configuration at the same angle of attack, for a similar blowing coefficient. Lift coefficients are almost the same $C_l \simeq 4.4$ whereas the elliptical shape airfoil is capable of achieving the same amount of lift with lower mass flow \dot{m}

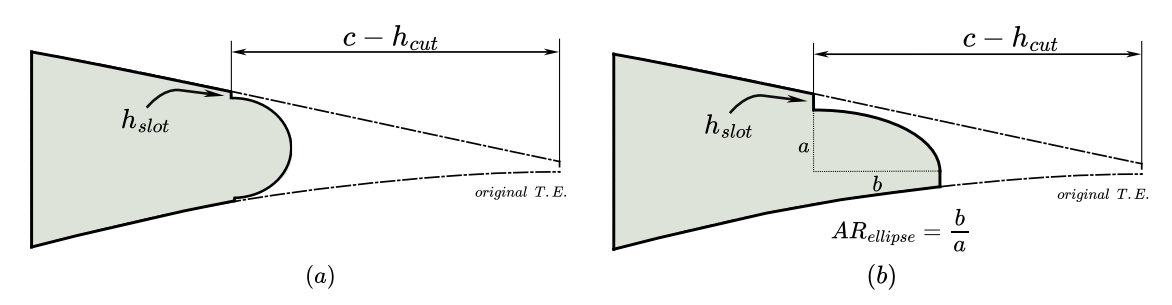
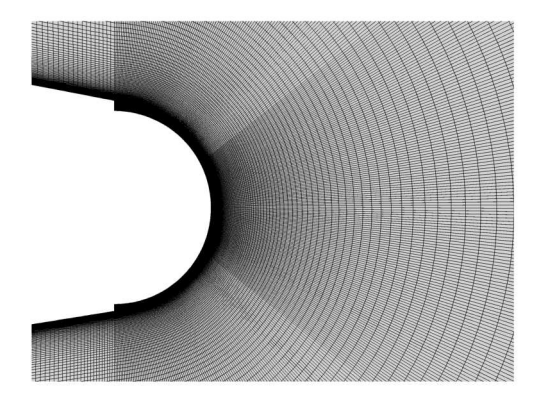


Figure 15. Sketch of T.E. geometrical definition for both (a) circular shape and (b) elliptical shape.

	A0	<i>A</i> 1	A2	B 0	<i>B</i> 1	<i>B</i> 2
h_{cut}	0.90	0.9	0.85	0.85	0.85	0.85
h_{slot}	0.2%	0.3%	0.3%	0.2%	0.3%	0.1%

Table 3. Preliminary geometry parameters for A-circular shape and B-elliptic shape with $\mathcal{R}=2$, referred to airfoil chord.



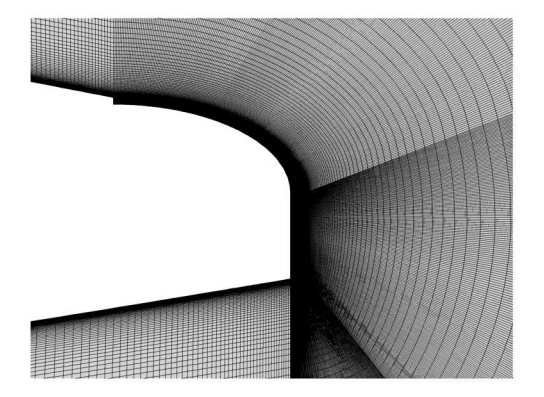


Figure 16. Structured mesh on A2 circular configuration.

Figure 17. Structured mesh on B0 ellipse configuration with aspect ratio $\mathcal{R} = 2$.

Lift coefficient comparisons between all the preliminary configurations are reported in figure 22 for different momentum coefficients at $\alpha=4$ deg. The elliptic configuration B0 seems to be better than the others. Airfoil B2 works only at lower C_{μ} because, due to the small jet slot, it reaches sonic conditions early, thus this geometry is not capable of exploiting the circulation control regime. Also, circular T.E.

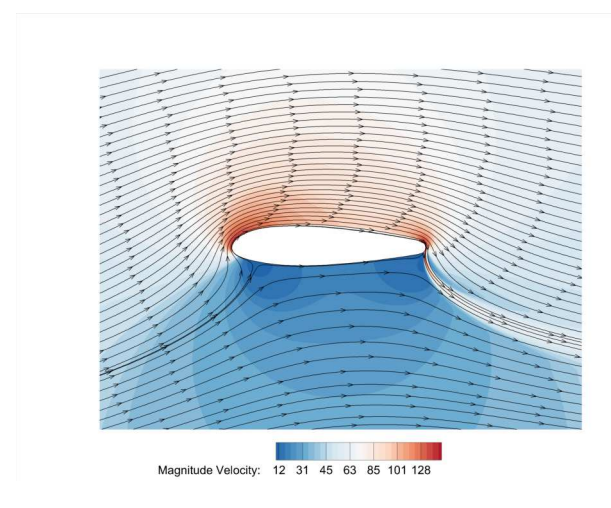


Figure 18. Velocity contour and streamline for A2 configuration, $C_u = 0.178$, $\alpha = 4$ deg, $C_l = 4.42$, $\dot{m} = 1$ kg/s

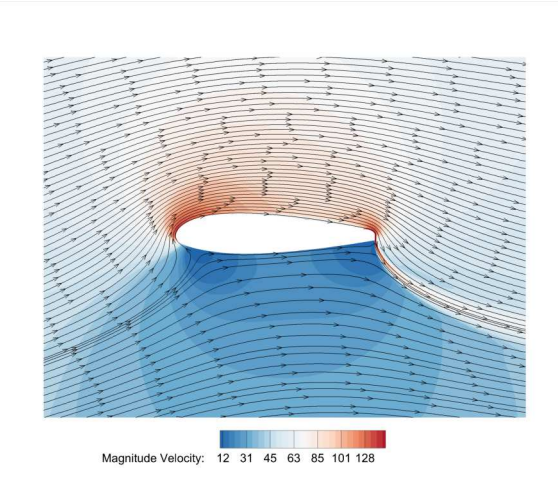


Figure 19. Velocity contour and streamline for B0 configuration, $C_u = 0.171$, $\alpha = 4$ deg, $C_l = 4.41$, $\dot{m} = 0.8$ kg/s

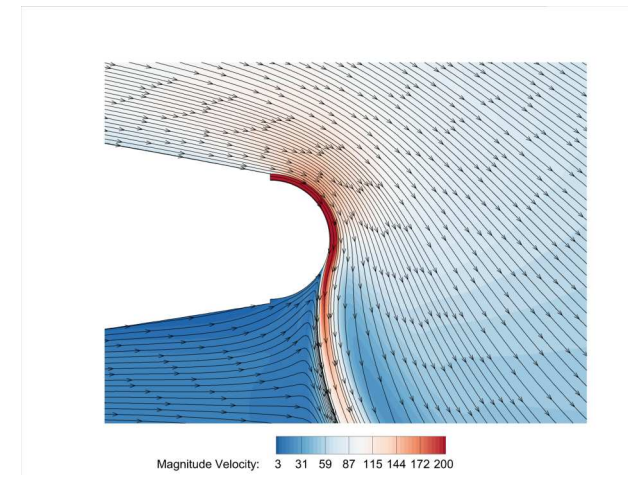


Figure 20. Velocity contour and streamline for A2 configuration, $C_{\mu}=0.178,~\alpha=4~deg,~C_{l}=4.42,~\dot{m}=1~kg/s$

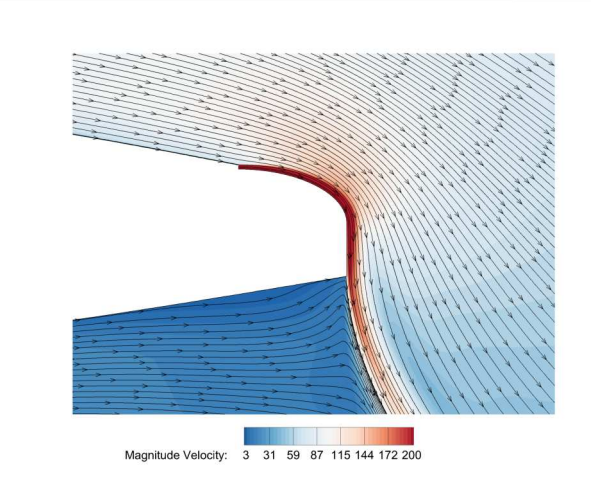


Figure 21. Velocity contour and streamline for B0 configuration, zoom at trailing edge, $C_{\mu}=0.171,~\alpha=4~deg,~C_{l}=4.41,~\dot{m}=0.8~kg/s$

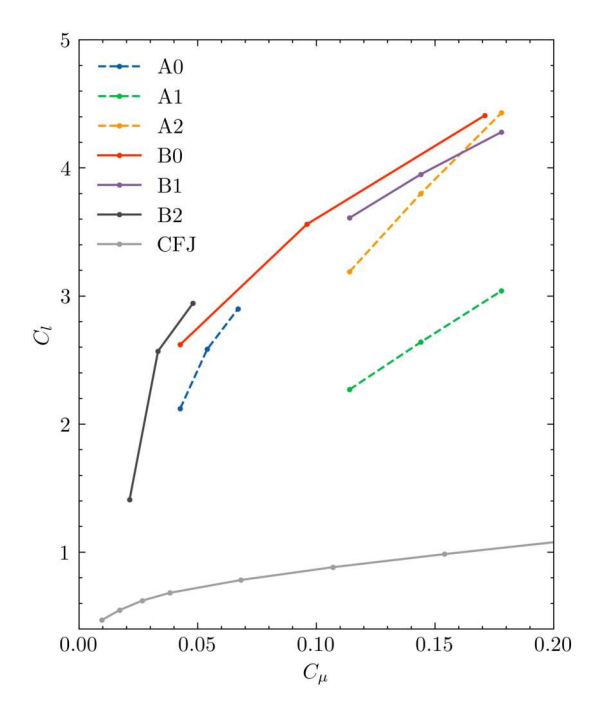
airfoil A2 seems to be promising although to have the same C_{μ} a higher mass flux must be provided. From the drag polar comparison depicted in figure 23, the A2 and B0 configurations seem to be better than the others. Must be noted that the drag reported in the latter figure is only the pressure and shear contribution without considering the thrust force given by momentum injection: for relatively high C_{μ} the system behaves as a propulsion system thus the total force along x aerodynamic axis component is negative and goes linear with the C_{μ} .

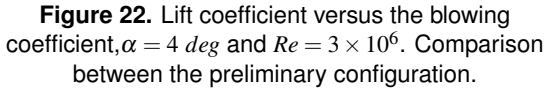
Also, a Co-Flow jet technology is analyzed, in order to assess its performance with respect to the configuration already characterized. Injection and suction slots are applied on the baseline geometry following the optimal criteria introduced by other studies.

$h_{slot,inj}$	$h_{slot,suc}$	θ_{inj}	θ_{suc}	x_{inj}	x_{suc}
0.005	0.01	24	9	0.06	0.75

Table 4. Co-Flow jet parameters applied on baseline airfoil referred to airfoil chord. h_{slot} are the sloth height, θ (in deg) refers to the incidence angle of jet inlet and outlet surface normal respect x direction, and x_{inj} individuate the position on the chord of the inlet as well as x_{suc} refers to the suction slot position.

Structured mesh is generated around the airfoil and RANS simulations are performed using SA turbulence modeling at several angles of attack and for different blowing levels. Figures 24 and 25 report respectively the velocity flow field contour around the airfoil with the blowing turned off and the one





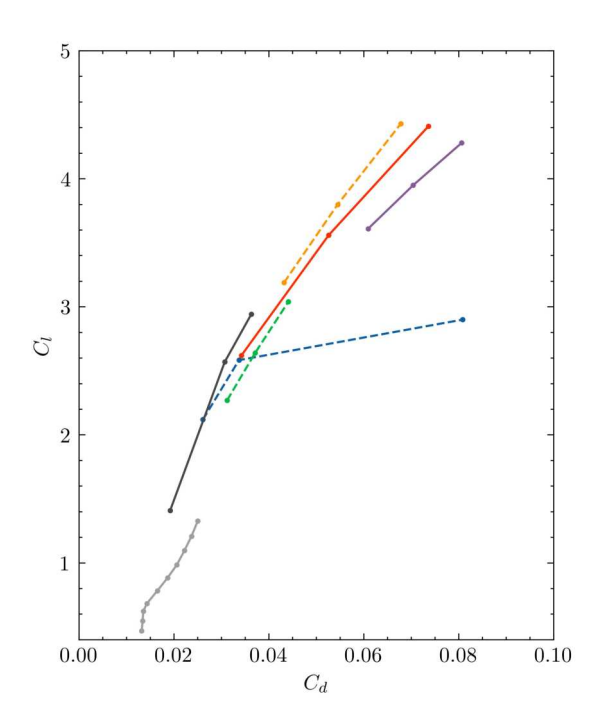


Figure 23. Lift coefficient versus the drag coefficient with different blowing coefficient, $\alpha=4~deg$ and $Re=3\times10^6$. Comparison between the preliminary configuration.

with a blowing coefficient $C_{\mu}=0.107$, both at $\alpha=10~deg$ and $U_{\infty}=50~m/s$. The lift coefficient versus the momentum coefficient is reported in the figure 22, compared with the Coanda airfoil. In figure 26 the Lift-to-gain Factor (LGF) is reported versus the momentum coefficient at $\alpha=4~deg$. An optimum LGF exists for $C_{\mu}=0.027$ meaning that this blowing level is the best way to expend energy to gain lift.

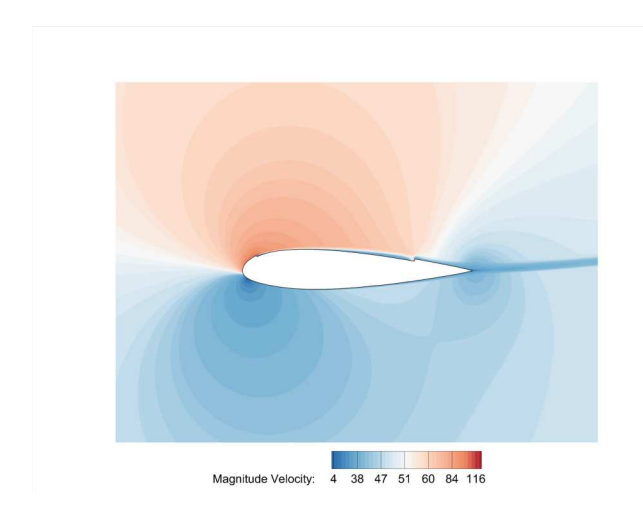


Figure 24. Velocity field contour around CFJ with no blowing, $\alpha=10~deg$ and $Re=3\times10^6$

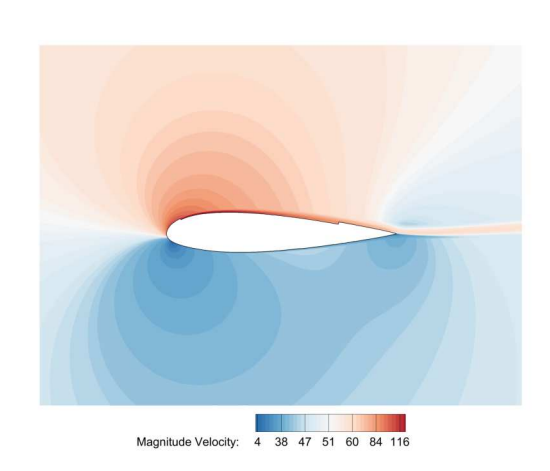


Figure 25. Velocity field contour around CFJ with $C_{\mu}=0.107,~\alpha=10~deg$ and $Re=3\times10^6$.

Once the preliminary study is done, a comparison between the most effective solutions is crucial to find the best device. Figures 27 and 28 report the lift coefficient and drag coefficient for the best-rounded shape trailing edge device (B0 configuration) and the CFJ, both in the condition of optimal LGF² at a target angle 4 deg respectively with $C_{\mu}=0.042$ and $C_{\mu}=0.027$. Are reported also the baseline airfoil, and the slotted flap airfoil results.

$$^{2}LGF = \frac{C_{l} - C_{l,baseline}}{C_{ll}}$$

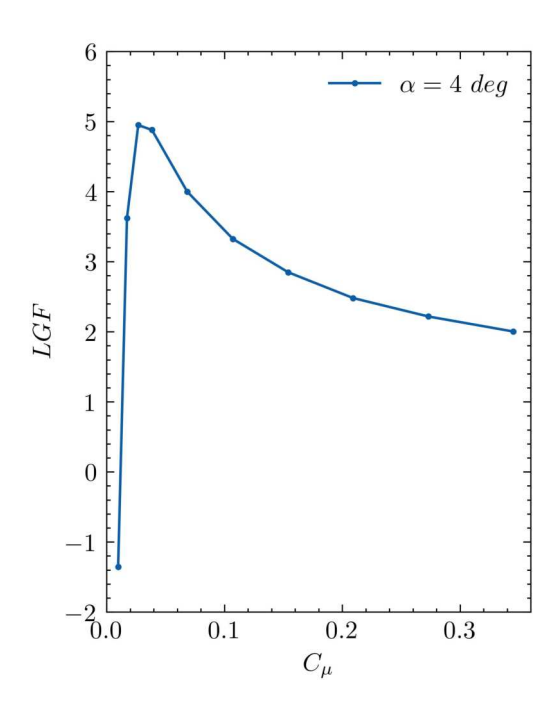


Figure 26. Lift to gain factor LGF of co-flow jet versus momentum coefficient at $\alpha = deg$

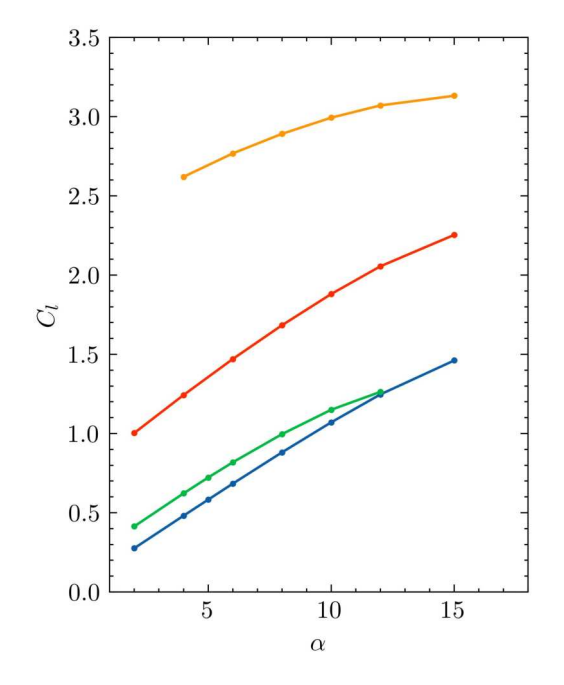


Figure 27. Lift coefficient versus angle of attack, and $Re = 3 \times 10^6$. Comparison between the preliminary configuration.

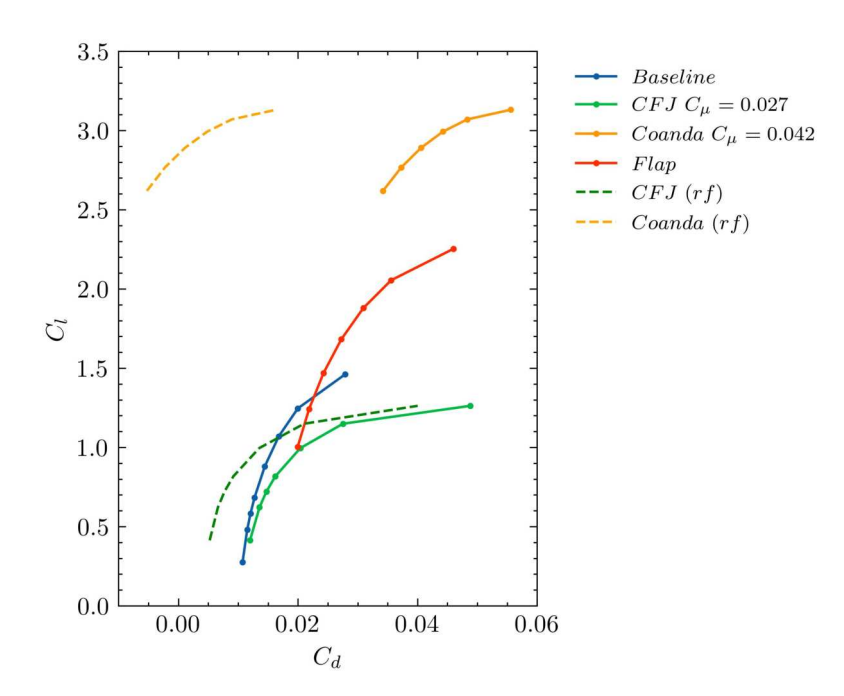


Figure 28. Lift coefficient versus the drag coefficient, $Re = 3 \times 10^6$. Comparison between the preliminary configuration. dotted lines indicate the inclusion of reaction forced due to the jet momentum injection.

3.1 Parametric Analysis

From the comparison between all the high-lift systems analyzed previously, the Coanda flap with an elliptical shape seems to have great potential due to its lifting capabilities. Thus, a parametric study is performed to assess which of the parameters that define completely the trailing edge geometry, better influence the aerodynamics. As depicted in figure 15, the main parameters used for the analysis of the elliptical trailing edge Coanda flap are the slot height h_{slot} , the cut length or the remaining airfoil length h_{cut} and the ellipse axis aspect ratio AR_{ell} .

A first study is conducted by fixing the ellipse aspect ratio and acting only on h_{cut} and h_{slot} within the range reported in table 5. Four values of aspect ratio are considered $(AR_{ell}=[0.7,1,2,3])$ and the flow condition are fixed $(U_{\infty}=50~m/s,~\alpha=4~deg)$ as well as solver option and turbulence modeling. Also, the blowing coefficient is fixed at one value $C_{\mu}=0.09$, in order to find the best shape, given fixed blowing effort. Parametric analysis is performed in the Ansys suite, by using the Response Surface Optimization tool. A Face Centered Central Composite Design is used as a Design type to spread and collocate the design points.

	lower bound	upper bound
h_{slot}	0.15	0.25
h_{cut}	75	85

Table 5. Upper and Lower bound considered in parametric analysis. Quantities expressed in percentage of the airfoil chord.

Figure 29 reports the lift coefficient contours to respect the two geometrical parameters for several ellipse aspect ratios: with limited aspect ratio, the maximum lift coefficient occurs within the minimum slot size and the minimum airfoil chord after cutting. The minimum slot height causes the maximum jet velocity at a fixed blowing coefficient, and the lower cut height increases the vertical surface on the back of the airfoil, making possible a more robust streamlines curvature control. When the aspect ratio becomes large, the slot opening where the jet is dumped is farther from the T.E. causing a loss of jet momentum before reaching the maximum of curvature. This is reflected in a plateau of lift coefficient, where the jet has become too weak to overcome the adverse pressure gradients thus it is not still capable of curving.

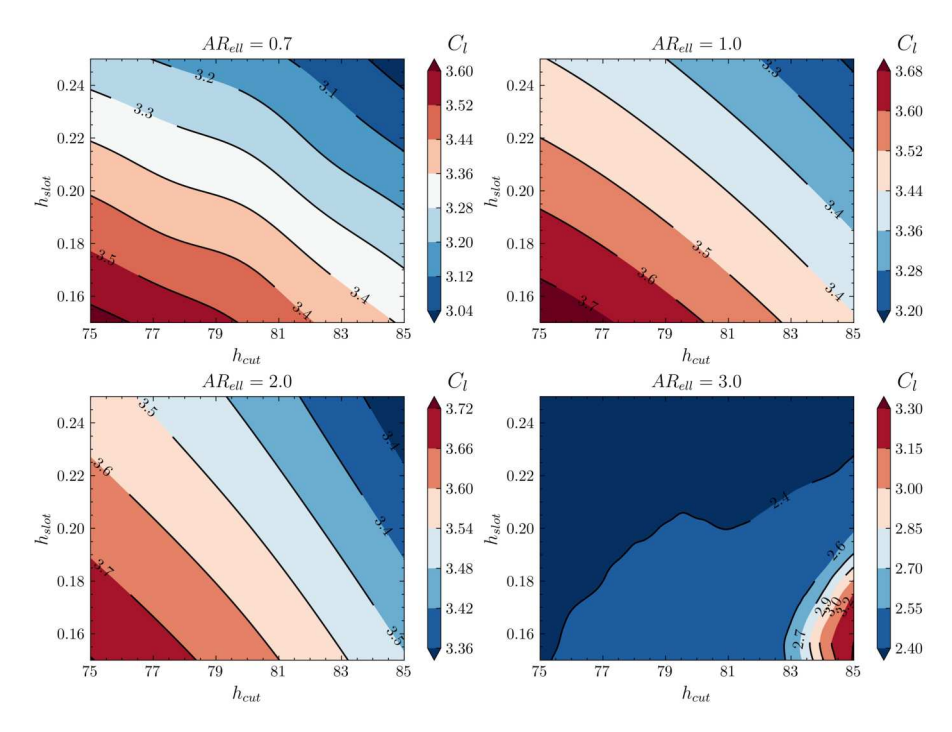


Figure 29. Lift coefficient contours at different ellipse aspect ratio, $C_{\mu}=0.09$, $\alpha=4$ deg and $U_{\infty}=50$ m/s

Figure 30 reports the Efficiency (C_l/C_d) without considering the reaction forces into C_d (thus the real

efficiencies are much higher). Even though the efficiency map seems to differ a lot by changing the aspect ratio, the absolute difference in each map is quite low. The most efficient configurations are the ones with a high aspect ratio ($AR_{ell}=3$), principally due to the lower drag associated with a more streamlined shape.

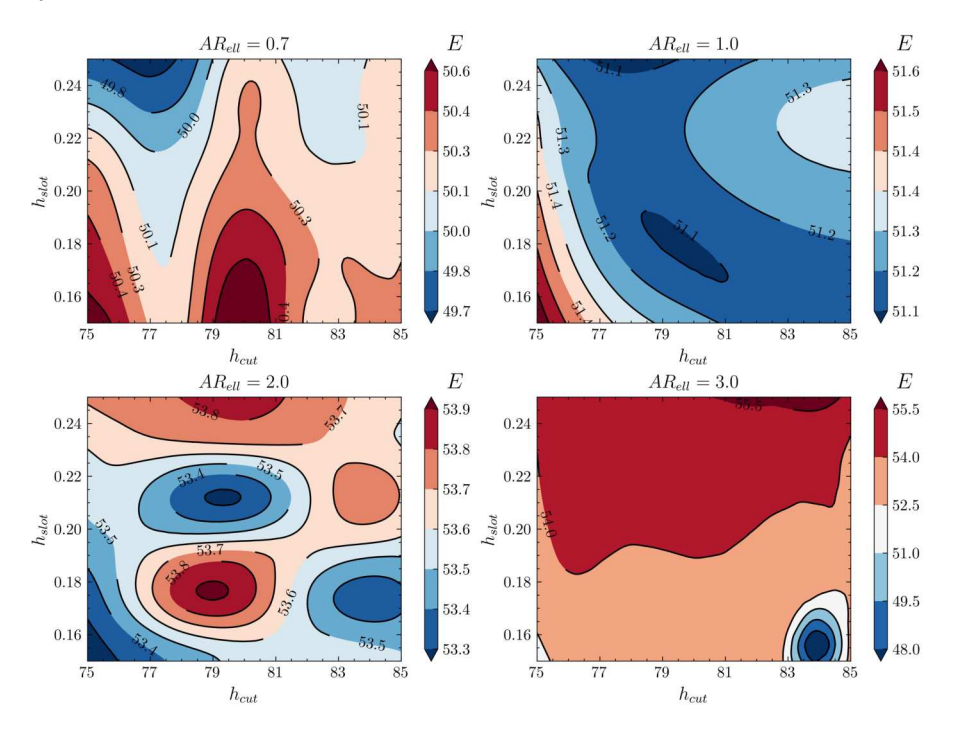
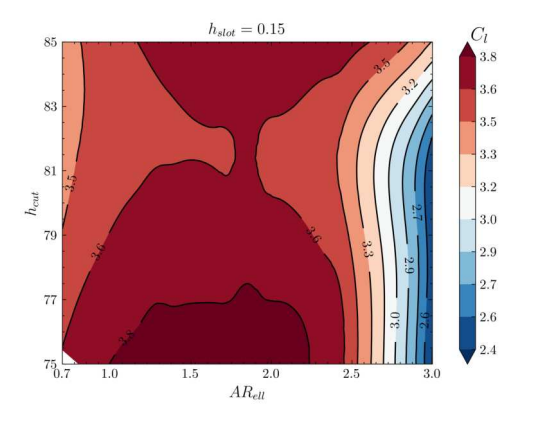
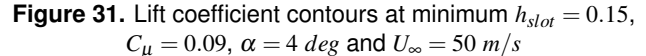


Figure 30. Lift to drag ratio *E* contours at different ellipse aspect ratio, $C_{\mu} = 0.09, \alpha = 4 \ deg$ and $U_{\infty} = 50 \ m/s$

A second analysis is performed considering all geometric parameters in the design exploration. The bound for h_{slot} and h_{cut} is the same as the ones reported in table 5 whereas the ellipse aspect ratio varies from 0.7 to 3.





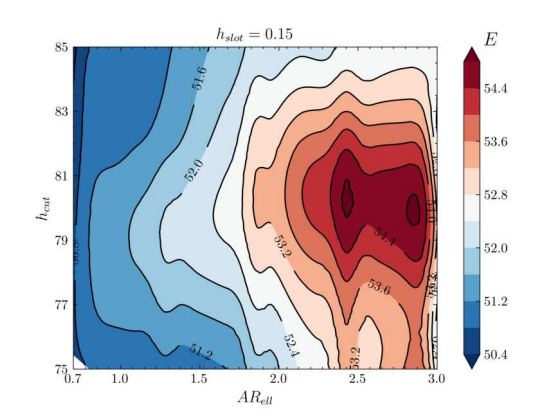


Figure 32. Efficiency contours at minimum $h_{slot} = 0.15$, $C_u = 0.09$, $\alpha = 4 \ deg$ and $U_{\infty} = 50 \ m/s$

Figure 31 and 32 reports respectively the lift coefficient and the efficiency contours versus AR_{ell} and h_{cut} at a fixed slot height h_{slot} , selected specifically its minim value 0.15 because topically correspond to the maximum lift coefficient. A local maximum lift coefficient ($C_l = 3.8$) exists for lower h_{cut} and medium aspect ratio, whereas the best configuration in terms of efficiency, occurs at a higher aspect ratio

The optimal configurations with different objectives are reported in table 6. Even though the efficiency of the best efficiency configuration and the best lift coefficient configuration are quite similar, the difference in lift coefficient is considerable ($\Delta C_l = 1.39$). The drag coefficient is always reported without the jet propulsion contribution. The real drag coefficient must account for the blowing coefficient, which in this case is quite high $C_\mu = 0.09$, leading to a total net drag coefficient becoming a thrust

coefficient (also with all the projection into aerodynamic axes).

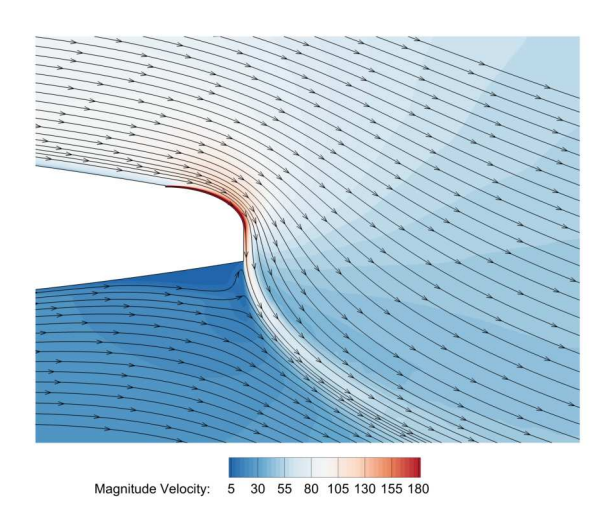


Figure 33. Velocity contours of the best lift coefficient configuration, $C_{\mu}=0.09,~\alpha=4~deg$ and $U_{\infty}=50~m/s$

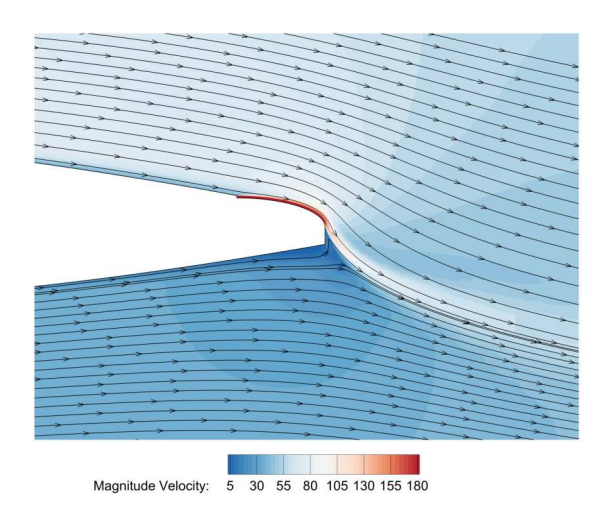


Figure 34. Velocity contours of the best efficiency configuration, $C_{\mu}=0.09,~\alpha=4~deg$ and $U_{\infty}=50~m/s$

Obj	h_{cut}	h_{slot}	AR_{ell}	C_l	C_d	Е	U_j/U_{∞}
$max(C_l)$	75	0.15	1.85	3.73	0.0701	53.2	5.4
max(E)	82	0.25	3	2.34	0.0427	54.8	4.2

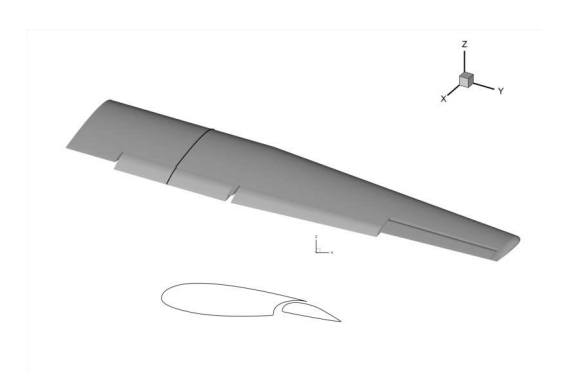
Table 6. Optimization results at fixed $C_{\mu}=0.9$ for different objective.

3.2 Wing Analysis

Once the best Coanda solution in terms of geometry and blowing level is determined in a two-dimensional study, a complete wing study is performed. To assess the performance of a CC wing obtained by the use of a Coanda airfoil as section, a wing with a classical slotted flap is used as a reference. The wing platform is similar, and the geometric details are reported in table 7. The geometries are depicted in figure 35 and figure 36, respectively slotted flap configuration and circulation control wing with airfoil B0. The extension of the blowing geometry is equal to the extension of the slotted flap of the conventional wing. An unstructured grid approach is used to generate a mesh with about 45 million points. RANS simulations are performed using the SA turbulence model in Fluent. The best blowing coefficient for B0 configuration is about 0.07, which corresponds to a total jet mass flow of $\dot{m} = 12~kg/s$. The aerodynamic forces computed for two angles of attack relative to the usual take-off operation are reported in table 8.

S	b	R	c_r	c_t	\bar{c}
$59 m^2$	27 m	12.3	2.555 m	$1.375 \ m$	$2.263 \ m$

Table 7. Wing geometric details



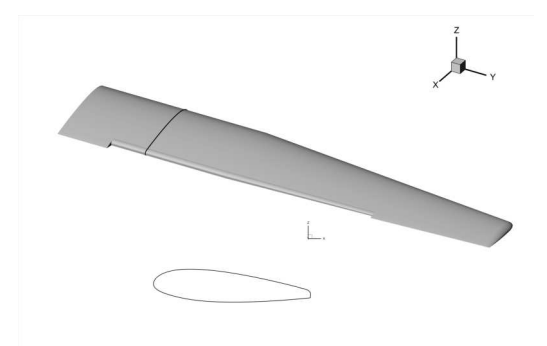


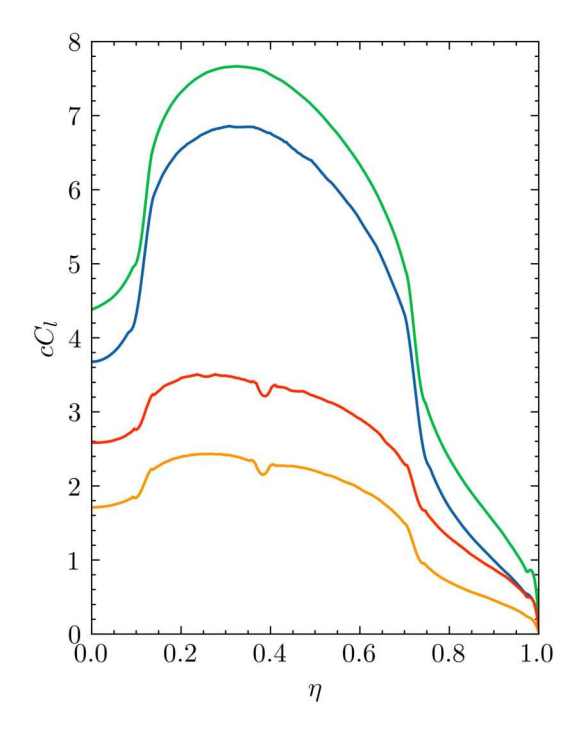
Figure 35. Wing with slotted flap in take-off configuration, $\delta_f = 15~deg$

Figure 36. Circulation Control wing geometry, section airfoil from configuration *B0*.

Lift and drag coefficients are calculated by the integration of pressure and shear forces on the wing surface, projected into the aerodynamic axis, without including the thrust effect given by the jet. Wing loading distribution for both the wing and angle of attack are reported in figure 37. The increasing of the angle of attack causes a load shifting to a higher value. The Coanda wing, for both angles of attack, has more lift capabilities while higher drag, most of it probably due to a larger change in load distribution at the flap compared to an equivalent elliptical loading (fig. 38). The higher lift coefficient per unit span is equivalent to a higher suction peak visible in the pressure coefficient on the upper surface of the wing (fig. 39). As the angle of attack increases, the region of suction will be more extended. The difference in wing loading distribution of the two high lift systems could be seen also by the x component of vorticity ξ_x in the wing wake: the effect of flap interruption is equivalent to a change of circulation thus the presence of vorticity beyond that zone. Circulation has a stronger span-wise derivative in the case of circulation control with respect to the slotted flap, causing higher vorticity in the wake. The wing tip vortices seem to be less strong than the one caused by the change in circulation due to the presence of flap or blowing.

	Slotted Flap Wing		CC Wing $C_{\mu}=0.07$		
	4 deg 8 deg		4 deg	8 deg	
C_L	0.76	1.18	2.07	2.40	
C_D	0.0338	0.0786	0.198	0.251	

 Table 8. Lift and drag coefficient of the sin with different high lift devices at different angles of attack.



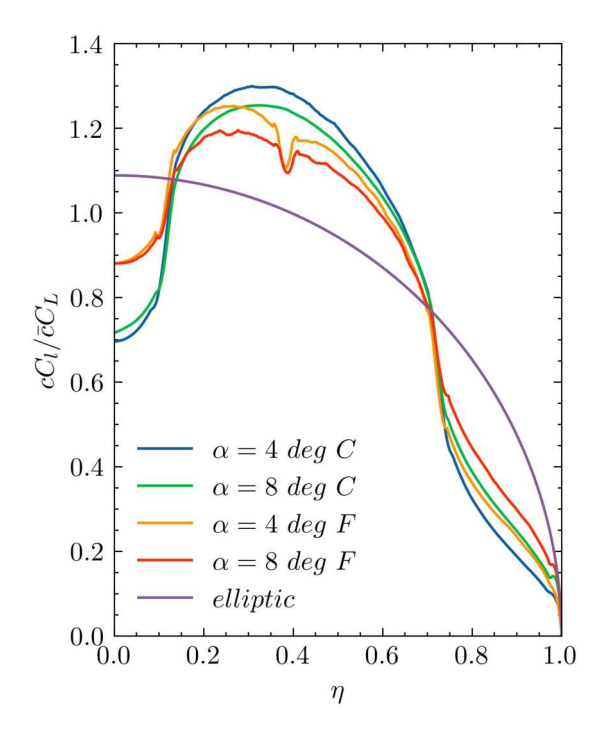


Figure 37. Wing loading distribution cC_l along semi-wing span $\eta = 2y/b$. Circulation Control and flapped wing at two angles of attack, $Re = 8.7 \times 10^6$.

Figure 38. Normalized wing loading versus semi-wing span compare with equivalent elliptic loading.'C' refers to the Coanda wing and 'F' to the flapped one.

4. Conclusion

Active flow control is seen as a viable solution to have a new generation of aircraft oriented to green aviation, lowering environmental impact, noise emissions, cost, and increasing reliability for UAM. Circulation Control wings have seen a lot of interest and development due to their high potentiality and flexibility. A numerical study is performed to assess the capability of circulation control technology starting with a two-dimensional airfoil. The absence of moving parts is adopted as a philosophy to mitigate the cost and weight reduction due to the presence of an actuation system. Several Coanda airfoil configurations are presented deriving from a systematic geometry parametrization. The best solution of the rounded trailing edge is compared with the novel Co-Flow jet and the classical slotted flap. Coanda airfoils have higher aerodynamic performances with respect to the other systems: they are capable of reaching high lift coefficients at lower angles of attack while lowering the total drag. This is useful from A STOL aircraft design perspective. A parametric study is performed on the elliptical trailing edge, to assess which geometrical or blowing parameter has more influence on the aerodynamics. Once the best solution between the ones analyzed, a three-dimensional numerical analysis is performed. A Circulation Control wing has more lifting capabilities than a slotted flap multielement wing (as suggested in 2D cases) while the strong variation of the wing loading distribution generates higher vorticity in the wake causing a higher drag coefficient. Although the circulation control wing could be seen as a distributed propulsion device, due to its lift capabilities, it generates very high lift-induced drag. This could be mitigated by optimizing the blowing distribution over the span, making the wing loading as regular as possible, and trying to mimic an elliptic one.

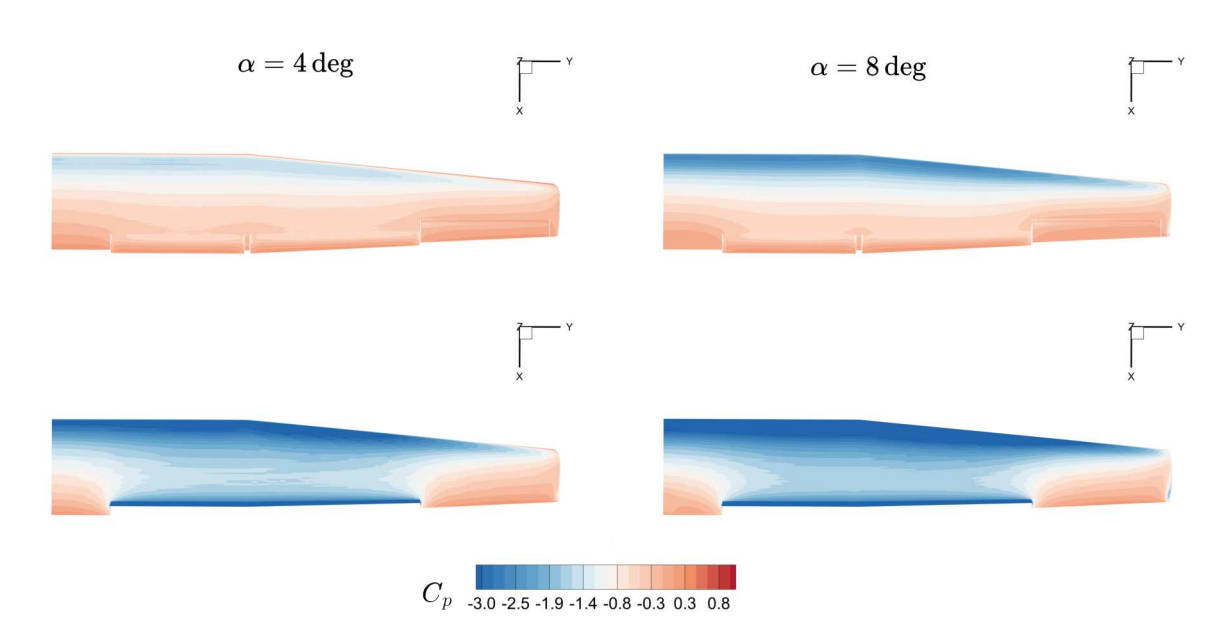


Figure 39. Pressure coefficient contour on the upper surface of two wings different high lift system, at $4 \deg$ and $8 \deg$, $Re = 8.7 \times 10^6$.

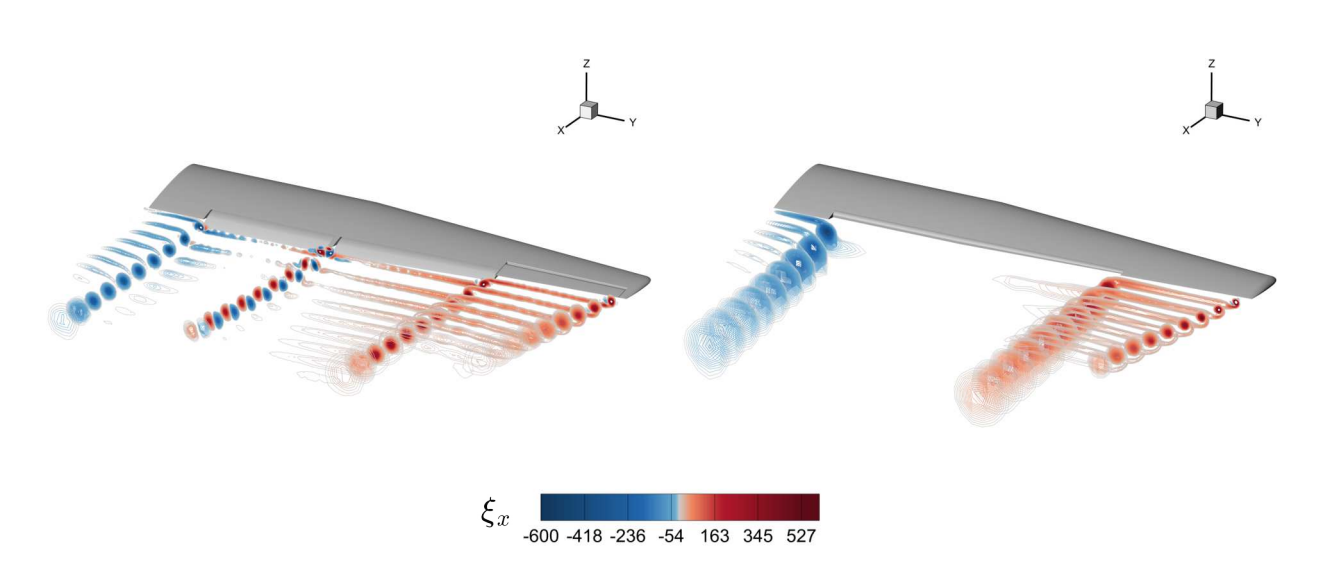


Figure 40. X component of vorticity contour line for slotted flap wing and circulation control wing with $C_{\mu}=0.07$, at $\alpha=4~deg$, $Re=8.7\times10^6$

5. Contact Author Email Address

mailto: piergiorgio.scavella@unina.it

6. Copyright Statement

The authors confirm that they, and/or their company or organization, hold copyright on all of the original material included in this paper. The authors also confirm that they have obtained permission, from the copyright holder of any third-party material included in this paper, to publish it as part of their paper. The authors confirm that they give permission, or have obtained permission from the copyright holder of this paper, for the publication and distribution of this paper as part of the ICAS proceedings or as individual off-prints from the proceedings.

7. Acknowledgements

This study was carried out within the MOST – Sustainable Mobility National Research Center and received funding from the European Union Next-GenerationEU (PIANO NAZIONALE DI RIPRESA E RESILIENZA (PNRR) – MISSIONE 4 COMPONENTE 2, INVESTIMENTO 1.4 – D.D. 1033 17/06/2022, CN00000023). This manuscript reflects only the authors' views and opinions, neither the European Union nor the European Commission can be considered responsible for them.

References

- [1] Frederico Afonso, Martin Sohst, Carlos MA Diogo, Simão S Rodrigues, Ana Ferreira, Inês Ribeiro, Ricardo Marques, Francisco FC Rego, Abdolrasoul Sohouli, Joana Portugal-Pereira, et al. Strategies towards a more sustainable aviation: A systematic review. *Progress in Aerospace Sciences*, 137:100878, 2023.
- [2] Rolf Radespiel and Wolfgang Heinze. Sfb 880: fundamentals of high lift for future commercial aircraft. *CEAS Aeronautical Journal*, 5(3):239–251, 2014.
- [3] Rolf Radespiel and Marco Burnazzi. Fundamentals in coanda flap design. In *Active Flow and Combustion Control 2014*, pages 101–114. Springer, 2015.
- [4] Christopher Courtin, Michael J Burton, Alison Yu, Patrick Butler, Parker D Vascik, and R John Hansman. Feasibility study of short takeoff and landing urban air mobility vehicles using geometric programming. In *2018 Aviation Technology, Integration, and Operations Conference*, page 4151, 2018.
- [5] CP Van Dam. The aerodynamic design of multi-element high-lift systems for transport airplanes. *Progress in Aerospace Sciences*, 38(2):101–144, 2002.
- [6] Mark D Moore. Wake vortex wingtip-turbine powered circulation control high-lift system. In *Proceedings* of the 2004 NASA/ONR Circulation Control Workshop, Part 2, 2005.
- [7] J. Wild. High-Lift Aerodynamics. CRC Press, 2022.
- [8] Peter K. C. Rudolph. High-lift systems on commercial subsonic airliners. 1996.
- [9] Meredith P. Viscous phenomena affecting high-lift systems and suggestions for future cfd development. high-lift systems on commercial subsonic airliners. AGARD CP 515, September 1993. p. 19-1–19-8.
- [10] J. K. Wimpress. Aerodynamic technology applied to takeoff and landing. *Annals of the New York Academy of Sciences*, 154(2):962–981, 1968.
- [11] Jonathan Kweder, Chad C Panther, and James E Smith. Applications of circulation control, yesterday and today. *International Journal of Engineering*, 4(5):411–429, 2010.
- [12] Apollo Milton Olin Smith. High-lift aerodynamics. Journal of Aircraft, 12(6):501-530, 1975.
- [13] Tianshu Liu. Evolutionary understanding of airfoil lift. Advances in Aerodynamics, 3(1):37, 2021.
- [14] MR Head. Entrainment in the turbulent boundary layer. 1958.
- [15] R Wille and H Fernholz. Report on the first european mechanics colloquium, on the coanda effect. *Journal of Fluid Mechanics*, 23(4):801–819, 1965.
- [16] Coanda Henri. Device for deflecting a stream of elastic fluid projected into an elastic fluid, September 1 1936. US Patent 2,052,869.
- [17] Robert J Englar and Robert M Williams. Design of a circulation control stern plane for submarine applications. *David W Taylor Naval ship Research and Development Center. Bethesda, MD*, 1971.
- [18] Robert J Englar, Marilyn J Smith, Sean M Kelley, and Richard C Rover III. Application of circulation control to advanced subsonic transport aircraft, part i-airfoil development. *Journal of Aircraft*, 31(5):1160–1168, 1994.
- [19] Ge-Cheng Zha and Craig Paxton. A novel airfoil circulation augment flow control method using co-flow jet. In 2nd AIAA flow control conference, page 2208, 2004.

- [20] Ge-Cheng Zha, Bruce F Carroll, Craig D Paxton, Clark A Conley, and Adam Wells. High-performance airfoil using coflow jet flow control. *AIAA journal*, 45(8):2087–2090, 2007.
- [21] Gecheng Zha, Yunchao Yang, Yan Ren, and Brendan McBreen. Super-lift and thrusting airfoil of coflow jet actuated by micro-compressors. In *2018 flow control Conference*, page 3061, 2018.
- [22] Yunchao Yang and Gecheng Zha. Improved delayed detached eddy simulation of super-lift coefficient of subsonic co-flow jet flow control airfoil. In 2018 AIAA Aerospace Sciences Meeting, page 0314, 2018.
- [23] Hong-Sik Im, Ge-Cheng Zha, and Bertrand PE Dano. Large eddy simulation of coflow jet airfoil at high angle of attack. *Journal of fluids engineering*, 136(2):021101, 2014.
- [24] ZHI Haolin, ZHU Zhenhao, LU Yujin, DENG Shuanghou, and XIAO Tianhang. Aerodynamic performance enhancement of co-flow jet airfoil with simple high-lift device. *Chinese Journal of Aeronautics*, 34(9):143–155, 2021.
- [25] Yunchao Yang and Gecheng Zha. Super-lift coefficient of active flow control airfoil: What is the limit? In 55th AIAA Aerospace Sciences Meeting, page 1693, 2017.
- [26] Alexis M Lefebvre and GeCheng Zha. Design of high wing loading compact electric airplane utilizing co-flow jet flow control. In *53rd AIAA aerospace sciences meeting*, page 0772, 2015.
- [27] Robert J Englar, Marilyn J Smith, Sean M Kelley, and Richard C Rover III. Application of circulation control to advanced subsonic transport aircraft. part ii-transport application. *Journal of Aircraft*, 31(5):1169–1177, 1994.
- [28] Tyler Ball, Scott Turner, and David D Marshall. Short takeoff performance using circulation control. 2008.
- [29] Warren Baker and Eric Paterson. Rans cfd simulation of a circulation-control foil: Validation of performance, flow feild, and wall jet. In *3rd AIAA Flow Control Conference*, page 3010, 2006.
- [30] Andreas Gross and HF Fasel. Coanda wall jet calculations using one-and two-equation turbulence models. *AIAA journal*, 44(9):2095–2107, 2006.
- [31] R Swanson, Christopher Rumsey, and Scott Anders. Progress towards computational method for circulation control airfoils. In 43rd AIAA Aerospace Sciences Meeting and Exhibit, page 89, 2005.
- [32] RC Swanson and CL Rumsey. Computation of circulation control airfoil flows. *Computers & Fluids*, 38(10):1925–1942, 2009.
- [33] Takafumi Nichino, Seonghyeon Hahn, and Karim Shariff. Les of high-reynolds-number coanda flow separating from a rounded trailing edge of a circulation control airfoil. In 8th International ERCOFTAC Symposium on Engineering Turbulence Modelling and Measurements (ETMM8), number ARC-E-DAA-TN1773, 2010.
- [34] Christopher L Rumsey and Takafumi Nishino. Numerical study comparing rans and les approaches on a circulation control airfoil. *International Journal of Heat and Fluid Flow*, 32(5):847–864, 2011.
- [35] Charles Novak, Kenneth Cornelius, and Ronalda Roads. Experimental investigations of the circular wall jet on a circulation control airfoil. In *25th AIAA Aerospace sciences meeting*, page 155, 1987.
- [36] Gregory Jones, Sally Viken, Anthony Washburn, Luther Jenkins, and Christopher Cagle. An active flow circulation controlled flap concept for general aviation aircraft applications. In 1st Flow control conference, page 3157, 2002.